Mechanics Research Communications 137 (2024) 104273

Contents lists available at ScienceDirect

Mechanics Research Communications

journal homepage: www.elsevier.com/locate/mechrescom

Bandgap structure of tensegrity mass–spring chains equipped with internal resonators

Luca Placidi [a], Julia de Castro Motta [b], Fernando Fraternali [b,*]

[a] International Telematic University Uninettuno, 00186 Rome, Italy
[b] Department of Civil Engineering, University of Salerno, 84084 Fisciano(SA), Italy

ARTICLE INFO

Keywords:
Maxwell chain
Frequency bandgaps
Internal resonance
Tensegrity structures

ABSTRACT

This work studies the dispersion relation of a Maxwell type mass–spring chain formed by lumped masses and the parallel arrangement of two different types of tensegrity prisms. Use is made of the Bloch–Floquet theory of discrete systems in association with a linearized model of the response of the tensegrity units under compression loading. Such a modeling is aimed at studying the propagation of compression waves under small perturbations of the initial equilibrium state of the system. For a given value of the cable's prestress, the tensegrity systems connecting the lumped masses react as elastic springs, which exhibit axial deformations accompanied by relative twisting rotations of the terminal bases. The twisting motion of the chain affects the expression of the kinetic energy, and is accounted for by introducing a suitable definition of equivalent masses. The bandgap structure of the analyzed system is analytically determined and numerical results are obtained for a chain formed by physical models tensegrity $\theta = 1$ prisms aligned in parallel with minimal tensegrity prisms. The given results highlight the highly tunable frequency bandgap properties of tensegrity mass–spring chains exhibiting internal resonance capabilities.

1. Introduction

Recent studies have shown that mass–spring chains with tensegrity architecture have the ability to control the speed of propagation of mechanical waves through the suitable tuning of internal and external prestress variables, in addition to more conventional stiffness control strategies [1,2]. It has also been shown that such systems can be employed to design linear mechanical metamaterials with tunable frequency bandgaps, when one examines dynamic excitations that induce small perturbation of the initial equilibrium state [3,4]. The frequency bandgap studies conducted so far in this area have mainly examined cases in which tensegrity prism units are in frictionless contact with the lumped masses, in order to exclude that the twisting motion of the bases of the prisms is transmitted to the masses [3], or cases in which the axial and twisting motions are uncoupled [4]. The coupling between axial and twisting motions has been analyzed in [2] within a study of the impulsive wave dynamics of chains of tensegrity prisms.

The present study contributes to the above research field by introducing the following main novelties: (i) the study of novel tensegrity mass–spring chains that feature tensegrity $\theta = 1$ prisms [5] placed in parallel with minimal tensegrity prisms; (ii) the inclusion of a perfect bonding condition between the tensegrity units and the lumped masses, which allows us to analyze coupled axial and twisting motions; (iii) the mechanical modeling of the bandgap response of such an unprecedented tensegrity chain, accounting for the resonance of the inner units. The analyzed system exhibits enhanced bandgap tuning properties, due to the presence of a considerably large number of geometry, prestress and mechanical variables. Such a rich design landscape paves the way to the formulation of novel, multiscale vibration protection systems featuring hierarchical architectures (refer, e.g., to [6] and references therein). The structure of the paper is as follows. Section 2 illustrates the topology of the Maxwell tensegrity chain and the kinematics of the analyzed units, which accounts for the coupling of longitudinal twisting motions and the definition of effective masses. The dispersion relation of the chain is derived in Section 3, via the Bloch–Floquet theory. Section 4 presents numerical simulations dealing with physical models of the analyzed system, while concluding remarks and directions for future work are given in Section 5.

2. Maxwell mass–spring chain with tensegrity architecture

Let us consider the tensegrity mass–spring chain illustrated in Fig. 1, which shows N tensegrity $\theta = 1$ prisms [5] (hereafter referred to as 'P_H prisms') that run in parallel with couples of minimal T3 tensegrity prisms equipped with three bars ('P_R prisms'). Lumped masses are

* Corresponding author.
E-mail addresses: luca.placidi@uninettunouniversity.net (L. Placidi), jdecastromotta@unisa.it (J. de Castro Motta), f.fraternali@unisa.it (F. Fraternali).

https://doi.org/10.1016/j.mechrescom.2024.104273
Received 21 December 2023; Received in revised form 1 March 2024; Accepted 4 April 2024
Available online 13 April 2024

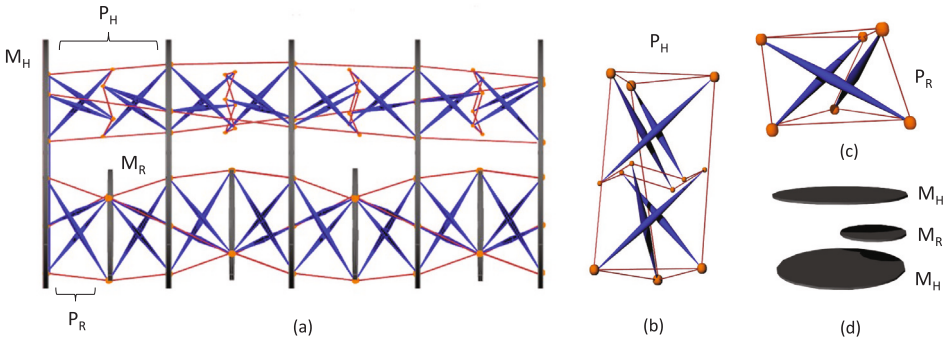

Fig. 1. (a) Illustration of a tensegrity chain formed by lumped masses, tensegrity $\theta = 1$ prisms and minimal T3 tensegrity prisms. (b–d) Close ups of a tensegrity $\theta = 1$ prism P_H (b); a T3 tensegrity prism P_r (c); and the disks forming the hosting masses M_H and the resonant masses M_R (d).

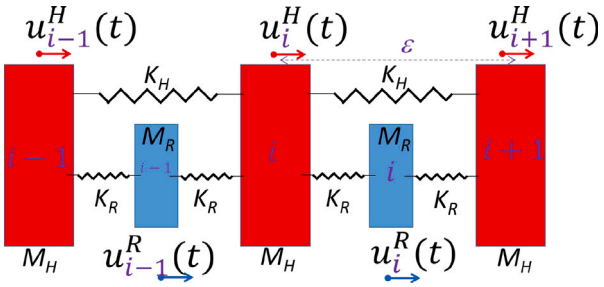

Fig. 2. A schematic picture of the Maxwell chain model.

alternated with the tensegrity units, which may consist of solid discs incorporated in the bases of the tensegrity prisms and/or point masses applied at the extremities of the bars (see Fig. 1). We employ a simplified modeling of the system shown in Fig. 1, which is aimed at studying its wave dynamics in the small displacement regime induced by small compression disturbances of the reference configuration. To this aim, we model the prism units as linear springs and describe the chain through the Maxwell model illustrated in Fig. 2. The latter is formed by a sequence of $2N + 1$ masses M_H and M_R. The $N + 1$ 'hosting masses' M_H are connected each other through N linear springs with stiffness constants K_H, while the N inner masses M_R are inserted between each couple of hosting masses and are supposed to act as 'resonant' bodies. Two linear springs with stiffness constants K_R connect the generic resonant mass with the two neighbor hosting masses. The stiffness constants K_H and K_R correspond to the values of the tangent stiffness that are respectively exhibited by the tensegrity prisms P_H and P_R in the reference configurations shown in Fig. 1 (see also Section 4). Let ε denote the overall longitudinal dimension of the unit cell, which is such that the distance between the generic mass M_H and the neighbor masses M_R is equal to $\varepsilon/2$. The position X_i of the generic mass in the reference configuration is given by $X_i = i\ \varepsilon/2$, with pair values of the index i corresponding to the positions of the $N + 1$ hosting masses M_H and odd values corresponding to the N resonant masses M_R. The displaced position of the generic hosting mass M_H is given by $x^H_i = X_i + u^H_i$, where the axial displacement u^H_i is a function of time t. Similarly, the displaced position of the generic resonant mass M_H is given by $x^R_i = X_i + u^R_i$, where u^R_i is the function of time describing the axial displacement of such a mass.

The reduction of the 3D tensegrity topology of Fig. 1 to the 1D Maxwell chain shown in Fig. 2 needs to account for the twisting motion that is produced by the relative rotations of the bases of the prism units about the axis of the chain [1,5]. Let us refer to a couple of hosting masses, which are connected by a P_H prism. The linearized response of the hosting tensegrity forming the ith cell, produced by a small compression disturbance of the reference configuration, gives rise to a counterclockwise relative rotation between the terminal bases

$$u^H_i - u^H_{i+1} = p^H\ (\vartheta^H_i\ -\ \vartheta^H_{i+1}), \qquad \forall i = 0, \dots, N-1 \tag{1}$$

where ϑ^H_i denotes the rotation of the ith hosting plate and p^H is a coupling parameter. Such a parameter can be easily computed by studying the kinematics of the tensegrity unit from the reference configuration, as we will show in Section 4. Eq. (1) tells us that a relative compression induces a relative rotation between the connected hosting plates. Similarly, the linearized response of the two resonant tensegrities forming the same unit cell gives rise to two relationships of the form

$$u^H_i - u^R_i = p^R\ (\vartheta^H_i\ -\ \vartheta^R_i), \qquad \forall i = 0, \dots, N-1, \tag{2}$$

$$u^R_i - u^H_{i+1} = p^R\ (\vartheta^R_i\ -\ \vartheta^H_{i+1}), \qquad \forall i = 0, \dots, N-1. \tag{3}$$

ϑ^R_i denoting the anticlockwise rotation of the ith resonance plate and p^R another positive additional kinematic parameter, which is pertinent to the P_R unit. Let us assume vanishing boundary conditions for both the hosting displacement u^H_N and the rotation ϑ^H_N (that is, $u^H_N = \vartheta^H_N = 0$). Under such assumptions, a straightforward manipulation of Eqs. (1)–(3) at $i = N - 1$ leads us to obtain

$$u^H_{N-1} = p^H\ \vartheta^H_{N-1} \tag{4}$$

$$u^R_{N-1} - u^H_{N-1} = p^R\ (\vartheta^R_{N-1} - \vartheta^H_{N-1}) \tag{5}$$

$$u^R_{N-1} = p^R\ \vartheta^R_{N-1} \tag{6}$$

The insertion of Eqs. (4) and (6) into (5) gives

$$\vartheta^H_{N-1}\left(p^R - p^H\right) = 0 \tag{7}$$

and we therefore conclude that it must result

$$p^H = p^R = p \tag{8}$$

in order to have a non vanishing solution with $\vartheta^H_{N-1} \neq 0$. Eq. (8) implies that the motions of the P_H and P_R units need to be suitably synced, in order to permit the propagation of mechanical waves in a tensegrity chain that exhibits coupled longitudinal and twisting motions. The use of Eq. (8) into Eqs. (1)–(3) finally leads us to the equations

$$u^H_i = p\ \vartheta^H_i, \quad \forall i = 0, \dots, N; \qquad u^R_i = p\ \vartheta^R_i, \quad \forall i = 0, \dots, N-1 \tag{9}$$

which imply that the kinematics of the system under consideration can be fully characterized by the axial displacements u^H_i and u^R_i. The kinetic energy $\mathcal{K}$ of the Maxwell chain is obtained by summing up the kinetic energies the unit each cells formed by the two masses M_H and M_R. The rotational inertia of such masses is related to moments of inertia $J_H = n_H\ M_H\ r^2_H$ and $J_R = n_R\ M_R\ r^2_R$ with respect to the axis of the chain. Here, r_H and r_R are the characteristic sizes (transverse with respect to the axis of the chain) of the above masses, and n_H and n_R are two scalar factors that depend upon their shapes. In the case of masses formed by circular disks with radii r_H and r_R (see Fig. 1), we trivially have $n_H = n_R = 1/2$. The analytic expression of $\mathcal{K}$ is as follows

$$\mathcal{K} = \frac{1}{2} M^{eq}_H (\dot{u}^H_N)^2 + \sum_{i=0}^{N-1} \frac{1}{2} \left[M^{eq}_H (\dot{u}^H_i)^2 + M^{eq}_R (\dot{u}^R_i)^2 \right] \tag{10}$$

where $\dot{u}_i^H$ and $\dot{u}_i^R$ are the axial velocities of the masses M_H and M_R, i.e. the derivatives with respect to time of u_i^H and of u_i^R, respectively, and $\dot{\vartheta}_i^H$ and $\dot{\vartheta}_i^R$ are the rotational velocities of the same masses. Eq. (10) makes use of the following 'equivalent masses'

$$M_H^{eq} = M_H\left(1+\frac{n_H r_H^2}{p^2}\right), \quad M_R^{eq} = M_R\left(1+\frac{n_R r_R^2}{p^2}\right) \tag{11}$$

which account for the coupling of longitudinal and twisting motion, under the assumption (8). Moving on to consider the external energy $\mathcal{U}^{ext}$ of the Maxwell chain, we observe that such a quantity is related to the longitudinal and rotational degrees of freedom via the external forces $F_{H,i}^{ext}$ and $F_{R,i}^{ext}$ and the external moments $\mathcal{M}_{H,i}^{ext}$ and $\mathcal{M}_{R,i}^{ext}$ acting on the chain. These quantities are the dual mechanical variables of the displacements u_i^H and u_i^R, and the rotations ϑ_i^H and ϑ_i^R, respectively. It is easy to show that it results in

$$\mathcal{U}^{ext} = \mathcal{F}_{H,N}^{ext,eq} u_N^H + \sum_{i=0}^{N-1}\left[\mathcal{F}_{H,i}^{ext,eq} u_i^H + \mathcal{F}_{R,i}^{ext,eq} u_i^R\right], \tag{12}$$

where the equivalent forces $\mathcal{F}_{H,i}^{ext,eq}$ and $\mathcal{F}_{R,i}^{ext,eq}$ have been introduced, though

$$\mathcal{F}^{ext,eq} = F_{H,i}^{ext} + \frac{\mathcal{M}_{H,i}^{ext}}{p}, \quad \mathcal{F}_{R,i}^{ext,eq} = F_{R,i}^{ext} + \frac{\mathcal{M}_{R,i}^{ext}}{p} \tag{13}$$

The final expression of the elastic internal energy of the chain is the following

$$\mathcal{U}_{int} = \sum_{i=0}^{N-1}\frac{1}{2}\left[K_R\left(\left(u_i^H-u_i^R\right)^2+\left(u_{i+1}^H-u_i^R\right)^2\right) + K_H\left(u_{i+1}^H-u_i^H\right)^2\right], \tag{14}$$

and one can define the *action* $\mathcal{A}$ of the system through [7]

$$\mathcal{A} = \int_{t_1}^{t_2}\left[\mathcal{K}-\mathcal{U}_{int}+\mathcal{U}_{ext}\right]dt \tag{15}$$

where t_1 and t_2 are two times at which the displacements u_i^H and u_i^R of all the masses are prescribed equal to given values $u_A^{H,i}$ and $u_A^{R,i}$, i.e. it results

$$u_i^H(t=t_A)=u_A^{H,i},\ u_N^H(t=t_A)=u_A^{H,N},\ u_i^R(t=t_A)=u_A^{R,i},\ A=1,2,\quad \forall i=0,\dots,N-1 \tag{16}$$

A variational principle

$$\delta\mathcal{A}=0, \quad \forall\delta u_i^H\in C_i^H, \quad \forall\delta u_N^H\in C_N^H, \quad \forall\delta u_i^R\in C_i^R, \quad \forall i=0,\dots,N-1 \tag{17}$$

is assumed to be valid for any admissible variations C_i^H of u_i^H and C_i^R of u_i^R, which allows us to obtain the equations of motion in the following form

$$M_H^{eq}\ddot{u}_i^H = F_{H,i}^{ext,eq} + K_R(u_i^R-u_i^H)+K_R(u_{i-1}^R-u_i^H) + K_H(u_{i+1}^H+u_{i-1}^H-2u_i^H), \tag{18}$$

$$M_R^{eq}\ddot{u}_i^R = F_{R,i}^{ext,eq} + K_R(u_i^H-u_i^R)+K_R(u_{i+1}^H-u_i^R) \quad \forall i=0,\dots,N-1, \forall t\in\mathbb{R} \tag{19}$$

It is worth noting that we were able to describe the articulated 3D tensegrity system shown in Fig. 1 through a simple 1D Maxwell chain model thanks to the reduction of the kinematics of each tensegrity prism unit to a single variable. This choice was made possible by the adoption of the compatibility assumptions (9), which relate the relative twisting rotations between the bases of the prisms to the relative axial displacements between the same members. The numerical simulations presented in Section 4 will show that such assumptions are reasonable in the small displacement regime, if one introduces an appropriate design of the state of prestress of the units.

3. Dispersion relation

By using the Bloch–Floquet theory of discrete periodic systems (see, e.g., [3]), we look for propagating harmonic waves of the following form

$$u_i^H = \mathrm{Re}\left\{u_0^H\exp\left[I\left(\omega t-k_w i\varepsilon\right)\right]\right\}, \quad u_i^R = \mathrm{Re}\left\{u_0^R\exp\left[I\left(\omega t-k_w i\varepsilon\right)\right]\right\} \tag{20}$$

where ω is the angular frequency, k_w is the wave number, I is the imaginary unit, Re denotes the real part operator and u_0^H and u_0^R are the two characteristic amplitudes of the propagating wave. In absence of external forces, it is easily shown that the insertion of Eq. (20) into the ordinary differential equations (18) and (19) yields the following dispersion relation between the frequency and the wave number of the propagating waves

$$\omega_{Mo,Ma}\left(k_w\right) = \sqrt{\frac{f(k_w)\pm\Delta_M\left(k_w\right)}{M_H^{eq}M_R^{eq}}} \tag{21}$$

where

$$f_M(k_w) = K_R(M_H^{eq}+M_R^{eq})+K_H M_R^{eq}(1-\cos k_w\varepsilon) \tag{22}$$

$$\Delta_M\left(k_w\right) = \sqrt{\left[f(k_w)\right]^2-2M_H^{eq}M_R^{eq}K_R(K_R+2K_H)(1-\cos k_w\varepsilon)} \tag{23}$$

In Eq. (21), the subscripts Mo and Ma denote the optic and acoustic branches of the dispersion relation, which are the periodic functions with period $2\pi/\varepsilon$ that are obtained by using the minus and plus sign in the term on the right side, respectively. Let us introduce the characteristic frequencies ω_R and ω_H of the masses M_R^{eq} and M_H^{eq}, through

$$\omega_R = \sqrt{2\frac{K_R}{M_R^{eq}}}, \quad \omega_H = \sqrt{2\frac{(K_H+\frac{1}{2}K_R)}{M_H^{eq}}} \tag{24}$$

For $k_w=0$, it is worth noting that the acoustic branch is zero, while the optic branch shows the nonzero frequency

$$\omega_{Mo}(0)=\omega_{Mo}^0=\sqrt{\frac{2K_R(M_H^{eq}+M_R^{eq})}{M_H^{eq}M_R^{eq}}} \tag{25}$$

On the other hand, for $k_w=\pi/\varepsilon$, both the acoustic and the optic branches show nonzero finite frequencies given by

$$\omega_{Ma}(\pi/\varepsilon)=\omega_{Ma}^{\pi}=\min(\omega_R,\sqrt{2}\omega_H), \quad \omega_{Mo}(\pi/\varepsilon)=\omega_{Mo}^{\pi}=\max(\omega_R,\sqrt{2}\omega_H) \tag{26}$$

Due to the periodic character of the acoustic and optic branches, one observes no wave solutions in correspondence to the following frequency bandgaps

$$\omega\in(\omega_1,\omega_2)\cup(\omega_3,\infty) \quad \Rightarrow \quad \textit{no wave solution} \tag{27}$$

where

$$\omega_1=\omega_{Ma}^{\pi}, \quad \omega_2=\min\left(\omega_{Mo}^0,\omega_{Mo}^{\pi}\right), \quad \omega_3=\max\left(\omega_{Mo}^0,\omega_{Mo}^{\pi}\right) \tag{28}$$

The upper bandgap in (27) prescribes no wave solutions for frequencies greater than ω_3. Besides, the lower frequency range $\omega\in(\omega_1,\omega_2)$ in (27) is usually referred to as the (primary) band gap of the Maxwell chain. Differently from standard biatomic chains (see, e.g., [3]), it is easily shown that the current Maxwell chain features frequency bandgaps also in absence of contrasts between masses (i.e., with $M_H^{eq}=M_R^{eq}=M^{eq}$) and stiffness of the springs ($K_H=K_R=K$), which are given by $\omega\in(\sqrt{2K/M^{eq}},\sqrt{4K/M^{eq}})\cup(\sqrt{6K/M^{eq}},\infty)$. The lower bound of the primary frequency bandgap ($\omega_1=\sqrt{2K/M^{eq}}$) corresponds to the resonant frequency of the inner mass $M^{eq}=M_R^{eq}$ connected to two springs with stiffness $K=K^R$. The upper bound of the same bandgap ($\omega_2=\sqrt{4K/M^{eq}}$) instead corresponds to the resonant frequency of the reduced mass $M^{eq}/2=M_H^{eq}M_R^{eq}/(M_H^{eq}+M_R^{eq})$ of the two-body system, which is formed by the two masses M_H^{eq} and M_R^{eq} connected to two springs with stiffness $K=K^R$.

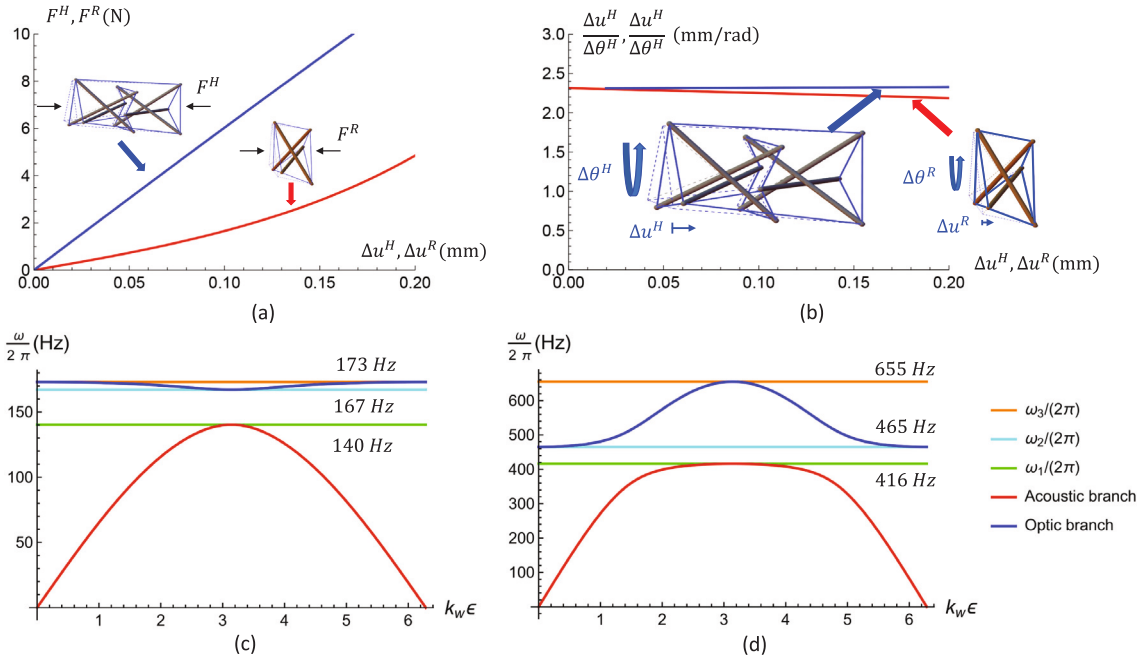

Fig. 3. (a) Force–displacement responses of the P_H and P_R prisms. (b) Relative axial displacement vs. twisting rotation laws exhibited by such units under small displacements from the reference configuration. (c) Dispersion relation of the tensegrity Maxwell chain with coupled longitudinal and twisting motions. (d) Dispersion relation of the chain featuring prisms that are free to slide against the lumped masses (no rotational motion of the masses).

4. Numerical examples

We hereafter examine physical realizations of the Maxwell chain model presented in the previous sections, which make use of micro-scale prisms P_H and P_R. The analyzed T3 prisms that form the P_R units exhibit a reference configuration characterized by a 5.5 mm height, equilateral triangular bases with 8.7 mm edge, cross-strings made of 6.1 mm long Spectra wires with 0.28 mm diameter and 5.48 GPa Young modulus, and Ti6Al4V bars with 0.8 mm diameter and 120 GPa Young modulus (see [8] for more details about such 3D-printable units). The terminal bases are rotated with respect to each other by an angle of twist of $5/6\pi$ (150 deg) in the reference configuration, which shows a 1% prestrain of the cross-strings. The $\theta = 1$ prisms forming the P_H units show a reference configuration with 11 mm height, equilateral triangular bases with 6.11 mm edge, cross-strings with 11.1 mm length, intermediate (or internal) strings with 3.05 mm length and 8.7 mm long bars. The sizes and materials of bars and strings are the same of those that characterize the T3 prisms. The terminal bases of the P_H prisms are subject to a relative angle of twist of 24.45 deg in the reference configuration, while the intermediate strings form an angle of 16.05 deg with the horizontal plane. The strings forming the terminal bases are subject to a 6.8×10^{-5} % prestrain. We refer the reader to [5] for the geometry of the tensegrity $\theta = 1$ prisms. For what concerns the masses, we use circular lead discs with 30 mm diameter and 2 mm thickness for the host masses ($M_H = 16.03$ g, $n_H = 1/2$), and lead discs with 15 mm diameter and 2 mm thickness for the resonant masses ($M_R = 4$ g, $n_R = 1/2$).

Let Δu^H and Δu^R denote the relative axial displacements between the bases of the P_H and P_R prisms, and let $\Delta\vartheta^H$ and $\Delta\vartheta^R$ denote the relative twisting rotations between such elements. Finally, let use the shorthand notations F^H and F^R for the external axial forces acting on the P_H and P_R prisms, respectively. Fig. 3(a) shows the axial force vs. axial displacement response of the analyzed units, while Fig. 3(b) depicts the laws relating the $\Delta u^{H,R}/\Delta\vartheta^{H,R}$ ratios with $\Delta u^{H,R}$, for small displacements from the reference configuration. Such plots have been computed by making use the path-following procedure illustrated in [5], assuming a rigid response of the terminal bases, due to the fact that such elements are incorporated in the lumped masses forming the chain. The results in Fig. 3(b) show that it can be reasonably assumed $p^H \approx p^R \approx 2.33$ mm/rad for the system under consideration. By computing the tangent stiffness coefficients of the force–displacement curves shown in Fig. 3(a), we estimate $K_R = 13.70$ N/mm, and $K_H = 61.04$ N/mm. A first chain model that we study features coupled longitudinal and twisting motions, as we have assumed in the previous sections. The equivalent masses characterizing such system amount to $M_H^{eq} = 349.51$ grams and $M_R^{eq} = 24.85$ grams, using Eq. (11), and one observes that such quantities are significantly larger that the physical masses M_H and M_R. Fig. 3(c) illustrates the dispersion relation of the present chain model, which shows a narrow optical branch and a primary bandgap for linear frequencies $\nu = \omega/(2\pi)$ between 140 Hz and 167 Hz (upper bandgap for frequencies larger than 173 Hz). A second chain model assumes that the P_H and P_R units are allowed to slide tangentially against the disk-masses (as in [3]), which determines the onset of a pure longitudinal motion of the M_H and M_R masses. As a result, the present chain model assumes $M_H^{eq} = M_H$ and $M_R^{eq} = M_R$. The dispersion relation of this second (uncoupled) chain model is illustrated in Fig. 3(d). One observes a thicker profile of the optical branch, as compared to the coupled chain model, and a primary bandgap for linear frequencies varying in between 416 Hz and 465 Hz (upper bandgap for frequencies greater than 655 Hz). It is also seen that the absence of rotational motion of the masses forming the chain determines the onset of bandgaps for frequencies markedly larger than those characterizing the coupled chain.

5. Concluding remarks

We were able to describe, for the first time, a complex and three-dimensional mass–spring system with tensegrity architecture through a simple Maxwell chain model with internal resonance features, thanks to the introduction of suitable compatibility equations between the twisting rotations and the axial displacements of the prism units. Recent studies on tensegrity bandgap systems have not explored the field in this direction, making the results of the present research ground breaking and worth pursuing in future work. Numerical examples concerned with physical systems formed by micro-scale units and masses, which can be conveniently fabricated through additive manufacturing

techniques [8], have highlighted that the onset of rotational motions of the host and resonant masses can be used to significantly reduce the amplitude of the bandgap frequencies. We address an experimental validation of the present study [9] and the development of discrete-to-continuum generalizations to future research, making use of continuum models endowed with both displacement and rotation kinematic variables.

CRediT authorship contribution statement

Luca Placidi: Writing – review & editing, Writing – original draft, Project administration, Investigation, Data curation, Conceptualization. **Julia de Castro Motta:** Writing – review & editing, Validation, Software, Investigation. **Fernando Fraternali:** Writing – review & editing, Writing – original draft, Investigation, Funding acquisition, Formal analysis.

Declaration of competing interest

The authors declare that they have no known competing financial interests or personal relationships that could have appeared to influence the work reported in this paper.

Data availability

Data will be made available on request.

Acknowledgments

This research has been funded under the National Recovery and Resilience Plan (NRRP), by the European Union – NextGenerationEU (“Ricerca finanziata dall’Unione europea – Next Generation EU”), within the project with grant number P2022CR8AJ (FF PI). This research has also been funded by the NextGenerationEU PRIN2022 research project with grant number 20224LBXMZ (FF PI). FF and JdCM also acknowledge the support by the Italian Ministry of Foreign Affairs and International Cooperation within the Italy-USA Science and Technology Cooperation Program 2023–2025, Project ”Next-generation green structures for natural disaster-proof buildings” (grant number US23GR15).

References

[1] W.O. Oppenheim, Geometric effects in an elastic tensegrity structure, J. Elasticity 59 (2000) 51–65.
[2] C. Davini, A. Micheletti, P. Podio-Guidugli, On the impulsive dynamics of T3 tensegrity chains, Meccanica 51 (2016) 2763–2776.
[3] A. Amendola, A. Krushynska, C. Daraio, N.M. Pugno, F. Fraternali, Tuning frequency band gaps of tensegrity metamaterials with local and global prestress, Int. J. Solids Struct. 155 (2018) 47–56.
[4] L. Placidi, F. Di Girolamo, R. Fedele, Bandgap structure of nested tensegrity mass–spring chains equipped with internal resonators, Mech. Res. Commun. 136 (2024) 104255.
[5] I. Mascolo, A. Amendola, G. Zuccaro, L. Feo, F. Fraternali, On the geometrically non-linear elastic response of class $\theta = 1$ tensegrity prisms, Front. Mater. 5 (2018) 16.
[6] V.F. Dal Poggetto, F. Bosia, M. Miniaci, N.M. Pugno, Band gap enhancement in periodic frames using hierarchical structures, Int. J. Solids Struct. 216 (2021) 68–82.
[7] F. Dell’Isola, L. Placidi, Variational Principles are a Powerful Tool also for Formulating Field Theories, Springer Vienna, 2011, pp. 1–15.
[8] A. Amendola, E.H. Nava, R. Goodall, I. Todd, R.E. Skelton, F. Fraternali, On the additive manufacturing, post-tensioning and testing of bi-material tensegrity structures, Compos. Struct. 131 (2015) 66–71.
[9] M. Laudato, L. Manzari, E. Barchiesi, F.Di. Cosmo, P. Göransson, First experimental observation of the dynamical behavior of a pantographic metamaterial, Mech. Res. Commun. 94 (2018) 125–127.